H^∞ repetitive control of DC-AC converters in micro-grids*

George Weiss, Qing-Chang Zhong†, Tim Green and Jun Liang
Dept. of Electrical & Electronic Engineering
Imperial College of Science, Technology and Medicine
Exhibition Rd., London, SW7 2BT, UK

Abstract

This paper proposes a voltage controller design method for DC-AC converters supplying power to a micro-grid, which is also connected to the power grid. This converter is meant to operate in conjunction with a small power generating unit. The design of the output voltage controller is based on H^∞ and repetitive control techniques. This leads to a very low harmonic distortion of the output voltage, even in the presence of nonlinear loads and/or a distorted grid voltage. The output voltage controller contains an infinite-dimensional internal model, which enables it to reject all periodic disturbances which have the same period as the grid voltage, and whose highest frequency components are up to approximately 1.5kHz.

Index Terms: Micro-grid, DC-AC power converter, voltage control, repetitive control, H^∞ control

1 Introduction

For economic, technical and environmental reasons, there is today a trend towards the use of small power generating units connected to the low-voltage distribution system in addition to the traditional large generators connected to the high-voltage transmission system [1]. Not only is there a change of scale but also a change of technology. Large generators are almost exclusively 50/60 Hz synchronous machines. Distributed power generators include variable speed (variable frequency) sources, high speed (high frequency) sources and direct energy conversion sources that produce DC. For example, wind-turbines are most effective if free to generate at variable frequency and so they require conversion from AC (variable frequency) to DC to AC (50/60 Hz) [2]; small gas-turbines with direct drive generators operate at high frequency and also require AC to DC to AC conversion [3]; photo-voltaic arrays require DC-AC conversion [4]. In all of these cases the same

*An early and abridged version of this work was presented at the IEEE Conf. on Decision and Control, Dec. 2002, Las Vegas, USA. This research was supported by the EPSRC under grant No. GR/N38190/1.

†Corresponding author, Tel: +44-20-7594 6295, Fax: +44-20-7594 6282, e-mail: zhongqc@ic.ac.uk, URL: http://www.ee.imperial.ac.uk/CAP.

basic inverter (DC to AC converter) will be used and needs to be controlled to provide high-quality supply waveforms to consumers.

There are several operating regimes possible for distributed generation. One such is the micro-grid in which the intention is that local consumers are largely supplied by local generation but that shortfalls or surpluses are exchanged through a connection to the public electricity supply system [5, 6]. The use of a micro-grid opens up the possibility of making the distributed generator responsible for local power quality in a way that is not possible with conventional generators [7].

Many of the loads connected to a distribution system or micro-grid are non-linear and create harmonically distorted current. The most common example is a linear load in series with a diode and with a DC-side capacitor. Many of the loads are also single-phase and so considerable zero-sequence distortion and a negative-sequence current component are expected. Because the grid has relatively high impedance at harmonic frequencies, the current distortion results in voltage distortion on the supply to adjacent customers. Allowing the converter in a generating unit to control the waveform shape of the micro-grid will allow better power quality to be achieved. Figure 1 shows the system to be controlled. The micro-grid loads contain both linear and distorting elements. In the representation of Figure 1, the loads have been lumped together into one linear load and a current sink which generates the harmonic components of the load current. The converter consists of a 4-wire, 3-phase inverter (IGBT bridge), an LC filter (to attenuate the switching frequency voltage components) and the controller. The micro-grid can be supplied solely by the local generator, or solely by the grid, or by both in combination, or the local generator can both supply the micro-grid and export power. Two isolators, S_c and S_g are provided to facilitate this and a grid interface inductor is provided to allow separation of the (sinusoidal) micro-grid voltage and the (possibly distorted) grid voltage and also to facilitate the control of the real and reactive power exchange between the micro-grid and the grid.

There are several aspects to the control of such a system:

- DC-link balancing,
- scheduling, connection, disconnection and synchronization of the micro-grid,
- micro-grid voltage control,
- power exchange control (between the micro-grid and the grid).

Some of the aspects of DC-link balancing, synchronization and power regulation have been described in earlier papers [8, 9, 10, 11]. This paper concentrates on the micro-grid voltage control. It is assumed that an outer control-loop will regulate power exchange between the micro-grid and grid by developing appropriate voltage references in terms of magnitude and phase angle. These reference voltages for the three phases of the micro-grid voltage are sinusoidal. It is then the task of the voltage controller to track accurately these reference voltages. This controller will be subject to disturbances which include non-sinusoidal currents, unbalanced current components, changes in load current, changes and distortions in the grid voltage, and changes in the DC-link voltage.

Several control options exist. Conventional PI regulators can be used and are widely reported in inverter control. In a rotating (dq) reference frame these regulators will seek

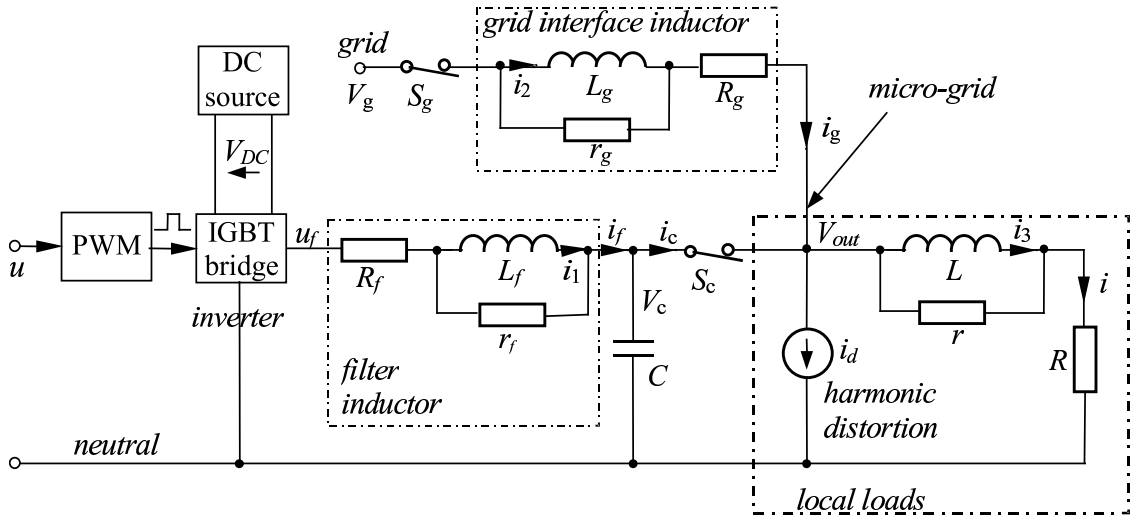

Figure 1: Single-phase representation of the system to be controlled. The local loads are represented by a single linear load in parallel with a harmonic distortion current source. The PWM block is designed such that if $|u(t)| < V_{DC}/2$ (no saturation), then the average of u_f over a switching period is the control input u.

to keep the dq voltage components at their DC reference values and suppress distortion that appears as higher frequency terms. These controllers can work well on balanced systems, but are not good at correcting unbalanced disturbance currents which are a common feature of distribution systems. Such controllers are commonly employed for balanced 3-phase motor loads. Regulators in a stationary reference frame can operate on a phase-by-phase basis and will have reasonable success at maintaining balanced voltages. The difficulty comes in designing a regulator with the correct gain against frequency characteristic to regulate the fundamental frequency and reject higher harmonic disturbances. PI regulators with their pole (infinite gain) at zero-frequency are not best suited to this task. A controller is required that has high gain at the fundamental and all harmonic frequencies of interest. Repetitive control [12, 13, 14, 15] is such a control technique. In this paper, we design the voltage controller based on the H^∞ repetitive control theory developed in [12], leading to a very low harmonic distortion of the micro-grid voltage even in the presence of nonlinear loads.

2 System modeling

The three-phase power system consists of the converter (including the IGBT bridge and LC filters), the local consumers, the grid interface inductor and the (external) power grid. We regard this system as three independent single-phase systems, as shown in Figure 1. This assumption may be inaccurate, with coupling between the phases present in some consumers, but the disturbances introduced can be rejected by the controller. The filter inductor and other inductors in the system include two parasitic resistances: a series resistor to model winding resistance and a parallel resistor to model core losses. The resistance

Table 1: Parameters of the system

parameter	value	parameter	value
R_f	0.053Ω	R_g	0.1Ω
L_f	1.3mH	L_g	0.3mH
r_f	30.5Ω	r_g	7Ω
R	5Ω	C	50μF
L	5mH	V_g	$230V,\ 50Hz$
r	500Ω	V_{DC}	$850V$

values we found from curve fitting experimental impedance data over the frequency range 50 Hz to 2 kHz.

The pulse-width-modulation (PWM) block is designed such that for $|u(t)| < 425$V, the local average of the bridge output voltage u_f equals u. This makes it possible to model the PWM block and the inverter with an average voltage approach. The PWM and inverter model is thus a simple saturated unity gain, where the saturation models the limit of the available DC-link voltage (± 425 V).

Our control objective is to maintain the micro-grid voltage V_{out} as close as possible to the given reference voltage V_{ref}. The two isolators S_c and S_g appearing in Figure 1 are needed in the start-up and shut-down procedures of the converter, which will not be discussed in this paper, but some of it is discussed in [8]. In this paper, the switches are considered to be closed. The parameters of the system are shown in Table 1. The switching frequency of the IGBT bridge is 10kHz.

We take the state variables as the currents of the three inductors and the voltage of the capacitor ($V_c = V_{out}$, since S_c is closed). The external input variables (disturbances and references) are i_d, V_g and V_{ref} and the control input is u. Thus,

$$x = \begin{bmatrix} i_1 \\ i_2 \\ i_3 \\ V_c \end{bmatrix}, \qquad \begin{bmatrix} w \\ u \end{bmatrix} \doteq \begin{bmatrix} i_d \\ V_g \\ V_{ref} \\ u \end{bmatrix}.$$

The state equations of the plant are

$$\dot{x} = Ax + \begin{bmatrix} B_1 & B_2 \end{bmatrix} \begin{bmatrix} w \\ u \end{bmatrix}, \tag{1}$$

where

$$A = \begin{bmatrix} -\frac{R_f r_f}{(R_f+r_f)L_f} & 0 & 0 & -\frac{r_f}{(R_f+r_f)L_f} \\ 0 & -\frac{R_g r_g}{(R_g+r_g)L_g} & 0 & -\frac{r_g}{(R_g+r_g)L_g} \\ 0 & 0 & -\frac{Rr}{(R+r)L} & \frac{r}{(R+r)L} \\ \frac{r_f}{(R_f+r_f)C} & \frac{r_g}{(R_g+r_g)C} & -\frac{r}{(R+r)C} & -(\frac{1}{R+r}+\frac{1}{R_f+r_f}+\frac{1}{R_g+r_g})\frac{1}{C} \end{bmatrix},$$

$$B = \left[\begin{array}{cc} B_1 & B_2 \end{array} \right] = \left[\begin{array}{ccc:c} 0 & 0 & 0 & \frac{r_f}{(R_f+r_f)L_f} \\ 0 & \frac{r_g}{(R_g+r_g)L_g} & 0 & 0 \\ 0 & 0 & 0 & 0 \\ -\frac{1}{C} & \frac{1}{(R_g+r_g)C} & 0 & \frac{1}{(R_f+r_f)C} \end{array} \right].$$

The output signals from the plant are the tracking error $e = V_{ref} - V_c$ and the current i_c, so that $y = \left[\begin{array}{c:c} e & i_c \end{array} \right]^T$. The output equations are

$$y = \left[\begin{array}{c} C_1 \\ C_2 \end{array} \right] x + \left[\begin{array}{cc} D_{11} & D_{12} \\ D_{21} & D_{22} \end{array} \right] \left[\begin{array}{c} w \\ u \end{array} \right],$$

where

$$C = \left[\begin{array}{c} C_1 \\ C_2 \end{array} \right] = \left[\begin{array}{cccc} 0 & 0 & 0 & -1 \\ \hdashline 0 & -\frac{r_g}{R_g+r_g} & \frac{r}{R+r} & \frac{1}{R+r} + \frac{1}{R_g+r_g} \end{array} \right],$$

$$D = \left[\begin{array}{cc} D_{11} & D_{12} \\ D_{21} & D_{22} \end{array} \right] = \left[\begin{array}{ccc:c} 0 & 0 & 1 & 0 \\ \hdashline 1 & -\frac{1}{R_g+r_g} & 0 & 0 \end{array} \right].$$

The corresponding plant transfer function is

$$\mathbf{P} = \left[\begin{array}{c|cc} A & B_1 & B_2 \\ \hline C_1 & D_{11} & D_{12} \\ C_2 & D_{21} & D_{22} \end{array} \right],$$

where we have used the compact notation now standard in control theory, see for example [16, 17], i.e., $\mathbf{P}(s) = C(sI - A)^{-1}B + D$.

3 Controller design

We will follow the H^∞ control-based design procedure for repetitive controllers proposed in [12], which uses additional measurement information from the plant. The block diagram of the control system is shown in Figure 2. The three external signals (the components of w) are assumed to be periodic, with a fundamental frequency of 50 Hz. The controller consists of an internal model and a stabilizing compensator. The internal model has an infinite sequence of pairs of conjugate poles of which about the first 30 are very close to the imaginary axis, around integer multiples of $2\pi \cdot 50j$, and the later ones are further to the left. The stabilizing compensator assures the exponential stability of the entire system. The error will then converge to a small steady-state error, see [12] for details.

As in [12], the internal model is obtained from a low-pass filter with transfer function

$$W(s) = \frac{\omega_c}{s + \omega_c}$$

with $\omega_c = 10000$ rad/sec, cascaded with a delay element with transfer function $e^{-\tau_d s}$, where τ_d is slightly less than the fundamental period $\tau = 20$msec:

$$\tau_d = \tau - \frac{1}{\omega_c} = 19.9 \text{ msec}.$$

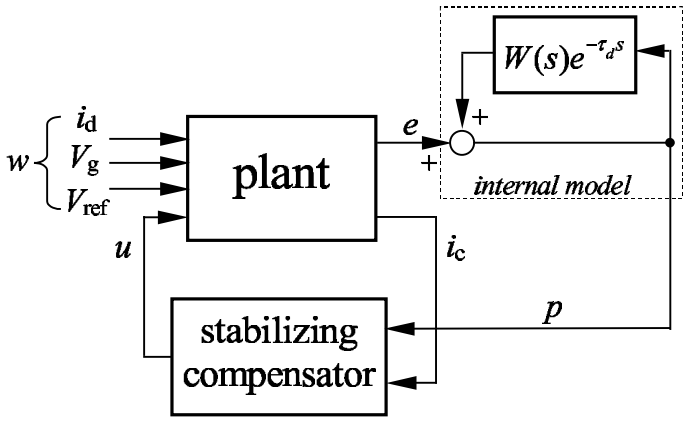

Figure 2: The robust repetitive control system. Here, w is the disturbance and e is the tracking error. The plant is the average model of the system from Figure 1.

After closing a positive unity feedback around this cascade connection, we obtain the internal model, as can be seen in Figure 2. The choice of ω_c is based on a compromise: for ω_c too low, only a few poles of the internal model will be close to the imaginary axis, leading to poor tracking and disturbance rejection at higher frequencies. For ω_c too high, the system is difficult to stabilize (a stabilizing compensator may not exist, or it may need unreasonably high bandwidth).

According to [12], the closed-loop system in Figure 2 is exponentially stable if the finite-dimensional closed-loop system from Figure 3 is stable and its transfer function from a to b, denoted $\mathbf{T}_{ba}$, satisfies $\|\mathbf{T}_{ba}\|_\infty < 1$. The intuitive explanation for this is that in the control system of Figure 2 a delay line is connected from the output b to the input a appearing in Figure 3. To make this interconnected system stable, by the small gain theorem, it is sufficient to make the gain from a to b less than 1 at all frequencies.

Thus, we have to design $\mathbf{C}$ (the transfer function of the stabilizing compensator) such that the above two conditions are satisfied. Moreover, we want to minimize $\frac{\gamma_0}{1-\gamma}$ while keeping $\gamma < 1$, where

$$\gamma_0 = \|\mathbf{T}_{ew}\|_\infty , \qquad \gamma = \|\mathbf{T}_{ba}\|_\infty .$$

Indeed, we know from [12, Section 5] that a small value for $\frac{\gamma_0}{1-\gamma}$ will result in a small steady-state error.

We formulate a standard H^∞ problem for the control system shown in Figure 3, where $\tilde{w} = [v_1 \; v_2 \; w]^T$ and, in terms of Laplace transforms,

$$\begin{bmatrix} \tilde{z} \\ \tilde{y} \end{bmatrix} = \tilde{\mathbf{P}} \begin{bmatrix} \tilde{w} \\ u \end{bmatrix}, \qquad u = \mathbf{C}\,\tilde{y}.$$

Here, ξ and μ are nonzero parameters whose choice gives us more freedom in the design. The small parameter μ is introduced to satisfy a rank condition needed to make the H^∞ problem solvable and W_u is a weighting function whose value at infinity, $D_u = W_u(\infty) \neq 0$, is also needed for a rank condition. The problem formulation here is a slight improvement over the one in [12], where W_u was a constant. The fact that W_u is

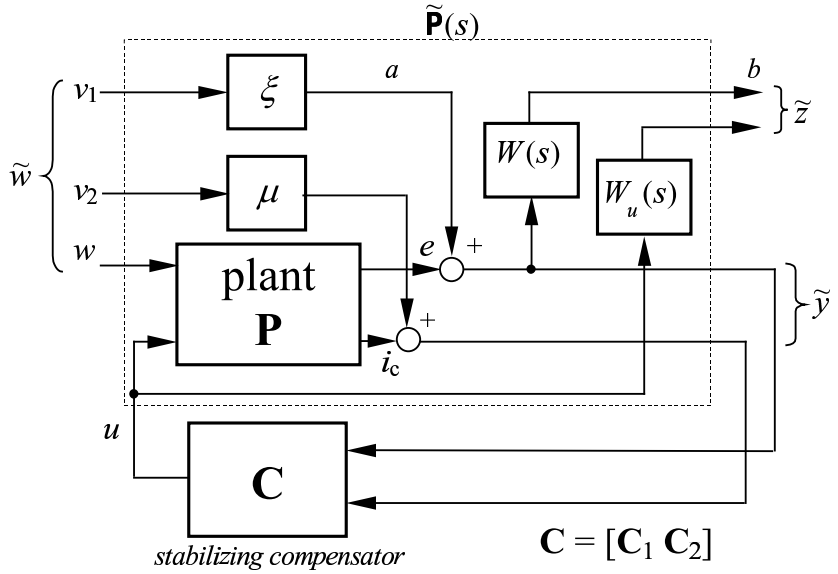

Figure 3: Formulation of the H^∞ control problem. This block diagram represents an auxiliary problem and it is not equivalent to the one shown in Figure 2.

---

frequency-dependent allows us to choose it as a high-pass filter. This has the effect of reducing the controller gains at high frequencies. The realizations of W_u and W are:

$$W_u = \left[\begin{array}{c|c} A_u & B_u \\ \hline C_u & D_u \end{array}\right], \quad W = \left[\begin{array}{c|c} A_w & B_w \\ \hline C_w & 0 \end{array}\right]$$

and the generalized plant $\tilde{\mathbf{P}}$ can be represented (see Appendix A) as

$$\tilde{\mathbf{P}} = \left[\begin{array}{ccc|ccc:c} A & 0 & 0 & 0 & 0 & B_1 & B_2 \\ B_w C_1 & A_w & 0 & B_w \xi & 0 & B_w D_{11} & B_w D_{12} \\ 0 & 0 & A_u & 0 & 0 & 0 & B_u \\ \hline 0 & C_w & 0 & 0 & 0 & 0 & 0 \\ 0 & 0 & C_u & 0 & 0 & 0 & D_u \\ \hdashline C_1 & 0 & 0 & \xi & 0 & D_{11} & D_{12} \\ C_2 & 0 & 0 & 0 & \mu & D_{21} & D_{22} \end{array}\right]. \tag{2}$$

Using the μ-analysis toolbox from MATLAB™, we can find a controller $\mathbf{C}$ which nearly minimizes the H^∞-norm of the transfer matrix from $\tilde{w}$ to $\tilde{z}$, $\mathbf{T}_{\tilde{z}\tilde{w}} = \mathcal{F}_l(\tilde{\mathbf{P}}, \mathbf{C})$. However, this is *not* our final objective. We denote the central sub-optimal controller for a given norm of $\mathbf{T}_{\tilde{z}\tilde{w}}$ by

$$\mathbf{C} = \left[\begin{array}{c|cc} A_c & B_{c1} & B_{c2} \\ \hline C_c & 0 & 0 \end{array}\right]$$

(note that its feedthrough matrix is equal to 0). After some manipulations (see Appendices B and C), we obtain the realizations of $\mathbf{T}_{ew}$ and $\mathbf{T}_{ba}$, respectively, as

$$\mathbf{T}_{ew} = \left[\begin{array}{cc|c} A & B_2 C_c & B_1 \\ B_{c1} C_1 + B_{c2} C_2 & A_c + (B_{c1} D_{12} + B_{c2} D_{22}) C_c & B_{c1} D_{11} + B_{c2} D_{21} \\ \hline C_1 & D_{12} C_c & D_{11} \end{array}\right], \tag{3}$$

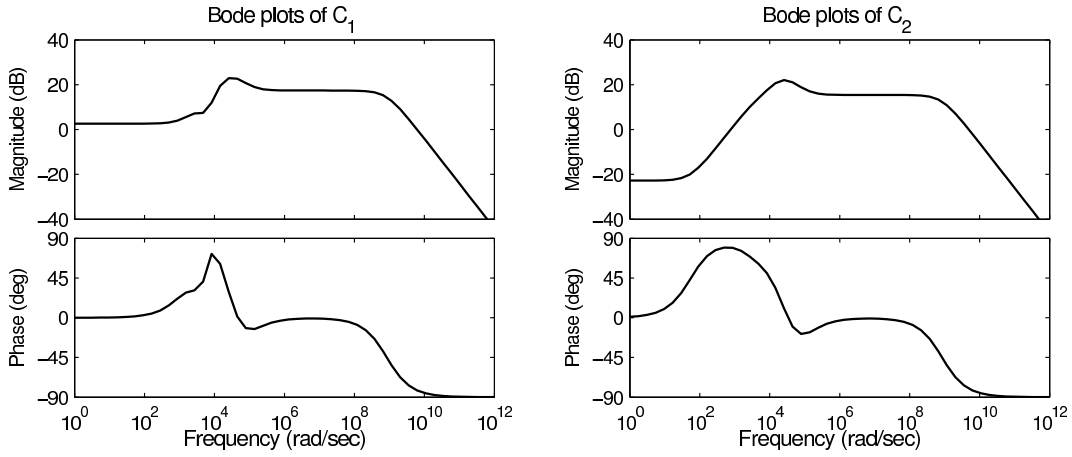

Figure 4: Bode plots of a nearly optimal controller $\mathbf{C}$ for the H^∞ problem shown in Figure 3. Note that it has a very large bandwidth, which is not realistic, given the switching frequency of 10kHz.

$$\mathbf{T}_{ba} = \left[\begin{array}{ccc|c} A & B_2C_c & 0 & 0 \\ B_{c1}C_1 + B_{c2}C_2 & A_c + (B_{c1}D_{12} + B_{c2}D_{22})C_c & 0 & B_{c1} \\ B_wC_1 & B_wD_{12}C_c & A_w & B_w \\ \hline 0 & 0 & C_w & 0 \end{array}\right]. \tag{4}$$

It is worth noting that the equations (2), (3) and (4) are valid for the general case, regardless of the dimension of the measurement vector, which here is the scalar i_c.

Using the parameters shown in Table 1, a nearly optimal controller, for which the Bode plots are shown in Figure 4, is obtained using $W_u(s) = \left[\begin{array}{c|c} -100000 & 1 \\ \hline -5000 & 0.05 \end{array}\right]$, $W(s) = \left[\begin{array}{c|c} -10000 & 10000 \\ \hline 1 & 0 \end{array}\right]$, $\xi = 14$ and $\mu = 0.5$ (these latter two were determined after an extensive search to minimize $\frac{\gamma_0}{1-\gamma}$ while keeping $\gamma < 1$). The Bode plots show that this controller is not realistic, because it has a very large bandwidth. In order to decrease the bandwidth, we do not minimize the H^∞-norm of $\mathcal{F}_l(\tilde{\mathbf{P}}, \mathbf{C})$ but find a central controller $\mathbf{C}$ such that $\left\|\mathcal{F}_l(\tilde{\mathbf{P}}, \mathbf{C})\right\|_\infty$ is less than a given positive number (which is larger than the minimal value). The Bode plots of an implementable controller are shown in Figure 5. We used this $\mathbf{C}$ as the stabilizing compensator in Figure 2, for the simulations.

4 Simulation results

The following simulations were done using Simulink in the Matlab™ environment (similar results were obtained also in PSCAD). The phase of the grid voltage is assumed to be 0° and the power control loop is open, i.e., the voltage reference signal is $V_{ref} = 325 \sin \omega t$ V. Thus, in steady state and if the grid is undistorted, there is no power exchange between the micro-grid and the grid. We have also run simulations with the power

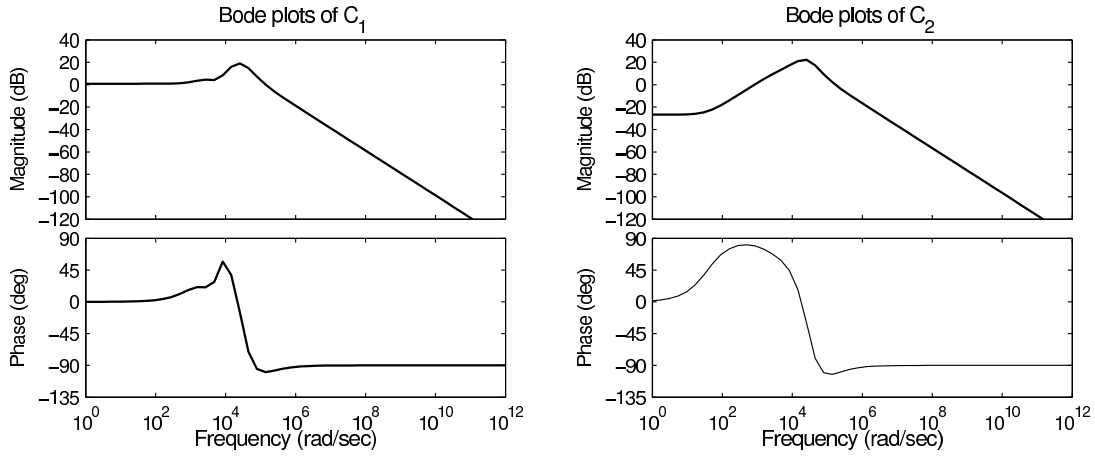

Figure 5: Bode plots of a more realistic controller $\mathbf{C}$

control loop working (see [8]), but here we omit those, since we do not want to burden this paper with the presentation of a power controller. From the point of view of voltage tracking, the results are similar, since the power control loop is much slower.

4.1 Nominal responses

Two simulations were conducted to assess the steady-state tracking performance of the system with the nominal load, with no disturbance current and an undistorted grid. The nominal load is shown in Figure 1, with the values of the components as in Table 1. The first simulation was conducted with the PWM block and the inverter modeled as a simple saturated gain, as described in Section 2. The output voltage and the tracking error, shown in Figure 6(a), demonstrate that the tracking error reduces to very small values after approximately 5 mains cycles. The steady-state error, which is less than 0.2V(peak), is shown in Figure 7(b). The second simulation used a detailed inverter model including a PWM block, switching at 10kHz. The response is shown in Figure 6(b). The results are similar but there is switching noise present that increases the steady-state tracking error which now has (short) peaks of approximately 20 V, see Figure 6(c). The controller is unable to suppress the switching noise, because it can only update the input to the pulse-width modulator once per carrier cycle.

Figure 7(b) shows the results of subjecting the plant to a disturbance current i_d, as shown in Figure 7(a), which has the typical shape of the distortion caused by a capacitive rectifier. The peaks of i_d are about half the nominal load current. As can be seen, the system has a good capability to reject such a disturbance.

4.2 The response to load changes

The load was changed to be a pure resistor of 50Ω (during the entire simulation), which represents about 10% of the load power used in Subsection 4.1. The PWM block and the inverter were still modeled as a saturation. The output voltage and the tracking error are

shown in Figure 8, with and without the disturbance current shown in Figure 7(a). No performance degradation can be observed from these figures (with respect to the nominal load).

A more involved simulation explored the transient responses when the load is changed from the nominal load to a pure resistor of 50Ω, see Figure 9. The load is changed at $t = 0.301$sec (when the load current is close to 0 so that the resulting spikes are small). The system reaches the steady state within 3 mains cycles and the dynamic error is less than 1 V. Here, we took $i_d = 0$.

4.3 The response to grid distortions

A typical grid voltage is flattened at its peaks. Here, a grid voltage of $V_g = 325 \sin \omega t - 32.5 \sin 3\omega t - 32.5 \sin 5\omega t$, as shown in Figure 10(a), is used as an example. The tracking error decays rapidly, as shown in Figure 10(b) and in steady state it becomes less than 0.5 V(peak). Although the external grid is extremely distorted, the local grid is very clean. In order to make it more clear, in this simulation, the disturbance i_d is set to 0 and the PWM block and the inverter are again modeled as a saturation.

5 Conclusions

A control structure has been proposed for a DC/AC power converter connected to a micro-grid with local loads and a public grid interface. The controller uses repetitive control on a per-phase basis in order to reject harmonic disturbances from non-linear loads or the public grid. An H^∞ design method has been used to ensure that the controller performs effectively with a range of local load impedances. The system has been modeled and tested in Matlab. The converter model includes a realistic switching frequency filter and a full model of the inverter PWM process. Our results have shown that, apart from the switching noise, the tracking of voltage references is accurate to within 0.2 V (for references of amplitude 325 V). The switching noise can have peaks of about 20 V, but there is nothing the controller can do to suppress this (high frequency) noise. If the load changes, the repetitive control loop converges and the tracking error becomes very small within approximately 3 mains cycles.

Appendix A: The realization of $\tilde{\mathrm{P}}$

This appendix contains the derivation of (2).

$$
\begin{aligned}
\tilde{y}_1 &= e + \xi v_1 \\
&= \xi v_1 + \left[\begin{array}{c|cc} A & B_1 & B_2 \\ \hline C_1 & D_{11} & D_{12} \end{array}\right] \begin{bmatrix} w \\ u \end{bmatrix} \\
&= \left[\begin{array}{c|cccc} A & 0 & 0 & B_1 & B_2 \\ \hline C_1 & \xi & 0 & D_{11} & D_{12} \end{array}\right] \begin{bmatrix} v_1 \\ v_2 \\ w \\ u \end{bmatrix},
\end{aligned}
$$

$$
\begin{aligned}
\tilde{y}_2 &= i_c + \mu v_2 \\
&= \left[\begin{array}{c|cc} A & B_1 & B_2 \\ \hline C_2 & D_{21} & D_{22} \end{array}\right] \left[\begin{array}{c} w \\ u \end{array}\right] + \mu v_2 \\
&= \left[\begin{array}{c|cccc} A & 0 & 0 & B_1 & B_2 \\ \hline C_2 & 0 & \mu & D_{21} & D_{22} \end{array}\right] \left[\begin{array}{c} v_1 \\ v_2 \\ w \\ u \end{array}\right],
\end{aligned}
$$

$$
\begin{aligned}
\tilde{z}_1 &= W(\xi v_1 + e) \\
&= \left[\begin{array}{c|c} A_w & B_w \\ \hline C_w & 0 \end{array}\right] \left[\begin{array}{c|cccc} A & 0 & 0 & B_1 & B_2 \\ \hline C_1 & \xi & 0 & D_{11} & D_{12} \end{array}\right] \left[\begin{array}{c} v_1 \\ v_2 \\ w \\ u \end{array}\right] \\
&= \left[\begin{array}{cc|cccc} A & 0 & 0 & 0 & B_1 & B_2 \\ B_w C_1 & A_w & B_w\xi & 0 & B_w D_{11} & B_w D_{12} \\ \hline 0 & C_w & 0 & 0 & 0 & 0 \end{array}\right] \left[\begin{array}{c} v_1 \\ v_2 \\ w \\ u \end{array}\right],
\end{aligned}
$$

$$
\tilde{z}_2 = W_u \cdot u = \left[\begin{array}{c|cccc} A_u & 0 & 0 & 0 & B_u \\ \hline C_u & 0 & 0 & 0 & D_u \end{array}\right] \left[\begin{array}{c} v_1 \\ v_2 \\ w \\ u \end{array}\right].
$$

Combine the above equations, then the realization of $\tilde{\mathbf{P}}$ is obtained as (2).

Appendix B: The realization of $\mathbf{T}_{ew}$

Assume $v_1 = 0$ and $v_2 = 0$, then $u = C_c x_c$, where x_c satisfies

$$\dot{x}_c = A_c x_c + B_{c1} e + B_{c2} i_c.$$

Substitute $u = C_c x_c$ into (1), then

$$\dot{x} = Ax + B_2 C_c x_c + B_1 w$$

and

$$
\begin{aligned}
e &= C_1 x + D_{12} C_c x_c + D_{11} w, \\
i_c &= C_2 x + D_{22} C_c x_c + D_{21} w.
\end{aligned}
$$

Furthermore,

$$\dot{x}_c = (A_c + B_{c1} D_{12} C_c + B_{c2} D_{22} C_c) x_c + (B_{c1} C_1 + B_{c2} C_2) x + (B_{c1} D_{11} + B_{c2} D_{21}) w.$$

Hence, the transfer matrix from w to e is

$$
\mathbf{T}_{ew} = \left[\begin{array}{cc|c} A & B_2 C_c & B_1 \\ B_{c1} C_1 + B_{c2} C_2 & A_c + (B_{c1} D_{12} + B_{c2} D_{22}) C_c & B_{c1} D_{11} + B_{c2} D_{21} \\ \hline C_1 & D_{12} C_c & D_{11} \end{array}\right].
$$

Appendix C: The realization of $\mathbf{T}_{ba}$

Assume $w = 0$ and $v_2 = 0$, then

$$\dot{x} = Ax + B_2 u,$$

$$e = C_1 x + D_{12} u,$$

$$i_c = C_2 x + D_{22} u$$

and $u = C_c x_c$, where

$$\begin{aligned} \dot{x}_c &= A_c x_c + B_{c1}(e + a) + B_{c2} i_c \\ &= A_c x_c + (B_{c1} C_1 + B_{c2} C_2) x + (B_{c1} D_{12} + B_{c2} D_{22}) C_c x_c + B_{c1} a, \end{aligned}$$

so that $e + a = C_1 x + D_{12} C_c x_c + a$. Hence, the transfer matrix from a to b is

$$\begin{aligned} \mathbf{T}_{ba} &= W \left[\begin{array}{cc|c} A & B_2 C_c & 0 \\ B_{c1} C_1 + B_{c2} C_2 & A_c + (B_{c1} D_{12} + B_{c2} D_{22}) C_c & B_{c1} \\ \hline C_1 & D_{12} C_c & 1 \end{array}\right] \\ &= \left[\begin{array}{c|c} A_w & B_w \\ \hline C_w & 0 \end{array}\right] \left[\begin{array}{cc|c} A & B_2 C_c & 0 \\ B_{c1} C_1 + B_{c2} C_2 & A_c + (B_{c1} D_{12} + B_{c2} D_{22}) C_c & B_{c1} \\ \hline C_1 & D_{12} C_c & 1 \end{array}\right] \\ &= \left[\begin{array}{ccc|c} A & B_2 C_c & 0 & 0 \\ B_{c1} C_1 + B_{c2} C_2 & A_c + (B_{c1} D_{12} + B_{c2} D_{22}) C_c & 0 & B_{c1} \\ B_w C_1 & B_w D_{12} C_c & A_w & B_w \\ \hline 0 & 0 & C_w & 0 \end{array}\right]. \end{aligned}$$

References

[1] N. Jenkins, R. Allan, P. Crossley, D. Kirschen, and G. Strbac, *Embedded generation*, IEE Power and Energy Series. IEE Books, 2000.

[2] Z. Chen and E. Spooner, "Grid power quality with variable speed wind turbines," *IEEE Trans. on Energy Conversion*, vol. 16, no. 2, pp. 148–154, 2001.

[3] M. Etezadi-Amoli and K. Choma, "Electrical performance characteristics of a new micro-turbine generator," in *IEEE Power Engineering Society Winter Meeting*, 2001, vol. 2, pp. 736–740.

[4] J.H.R. Enslin, M.S. Wolf, D.B. Snyman, and W. Swiegers, "Integrated photovoltaic maximum power point tracking converter," *IEEE Trans. Industrial Electronics*, vol. 44, no. 6, pp. 769 –773, 1997.

[5] R.H. Lasseter, "MicroGrids," in *Proc. of the IEEE Power Engineering Society Winter Meeting*, 2002, vol. 1, pp. 305–308.

[6] G. Venkataramanan and M. Illindala, "Microgrids and sensitive loads," in *Proc. of the IEEE Power Engineering Society Winter Meeting*, 2002, vol. 1, pp. 315–322.

[7] T.C. Green and M. Prodanović, "Control of inverter-based micro-grids," submitted to Electric Power Systems Research, special issue on Distributed Generation, 2003.

[8] J. Liang, T. Green, G. Weiss, and Q.-C. Zhong, "Decoupling control of the active and reactive power for a grid-connected three-phase DC-AC inverter," submitted to ECC'03, Cambridge, UK, 2003.

[9] Q.-C. Zhong and G. Weiss, "H^∞ control of the neutral leg for 3-phase 4-wire DC-AC converters," Submitted to IEEE Trans. Ind. Electron., 2002.

[10] Q.-C. Zhong, T. Green, J. Liang, and G. Weiss, "H^∞ control of the neutral leg for 3-phase 4-wire DC-AC converters," in *Proc. of The 28th Annual Conference of the IEEE Industrial Electronics Society (IECON'02)*, Seville, Spain, November 2002.

[11] J. Liang, T. Green, G. Weiss, and Q.-C. Zhong, "Evaluation of repetitive control for power quality improvement of distributed generation," in *Proc. of the 33rd IEEE Annual Power Electronics Specialists Conference*, Queensland, Autralia, June 2002, vol. 4, pp. 1803 –1808.

[12] G. Weiss and M. Hafele, "Repetitive control of MIMO systems using H^∞ design," *Automatica*, vol. 35, no. 7, pp. 1185–1199, 1999.

[13] Y. Yamamoto, "Learning control and related problems in infinite-dimensional systems," in *Essays on control: Perspectives in the theory and its applications*, H. Trentelman and J. Willems, Eds., pp. 191–222. Boston: Birkhäuser, 1993.

[14] K.L. Zhou, D. Wang, and K.-S. Low, "Periodic errors elimination in CVCF PWM DC/AC converter systems: repetitive control approach," *IEE Proc.Control Theory Appl.*, vol. 147, no. 6, pp. 694–700, 2000.

[15] K.L. Zhou and D. Wang, "Digital repetitive learning controller for three-phase CVCF PWM inverter," *IEEE Trans. Industrial Electronics*, vol. 48, no. 4, pp. 820–830, 2001.

[16] K. Zhou and J.C. Doyle, *Essentials of Robust Control*, Prentice-Hall, Upper Saddle River, N.J., 1997.

[17] M. Green and D.J.N. Limebeer, *Linear Robust Control*, Prentice-Hall, Englewood Cliffs, NJ, 1995.

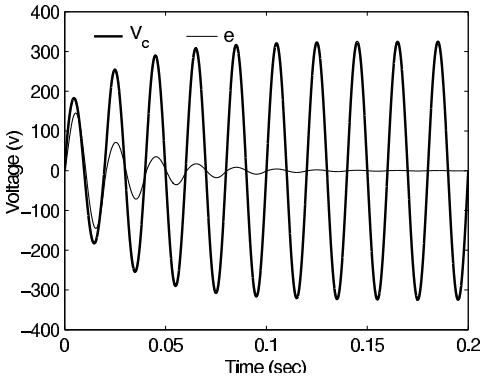

(a) With the PWM block and the inverter modeled as a simple saturation

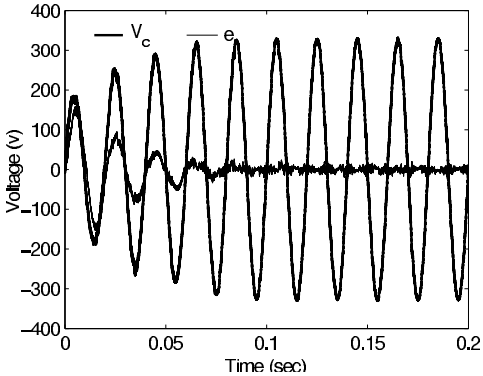

(b) With a detailed (not average) model of the PWM block and the inverter ($f_s = 10$kHz)

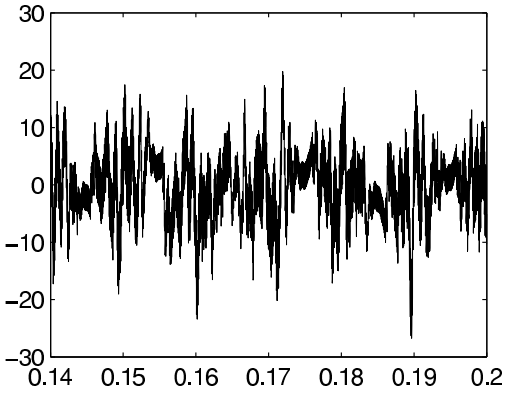

(c) The steady-state tracking error simulated with a detailed model of the PWM block and the inverter

Figure 6: The output voltage V_c and the tracking error e, without a current disturbance ($i_d = 0$) and with the nominal load.

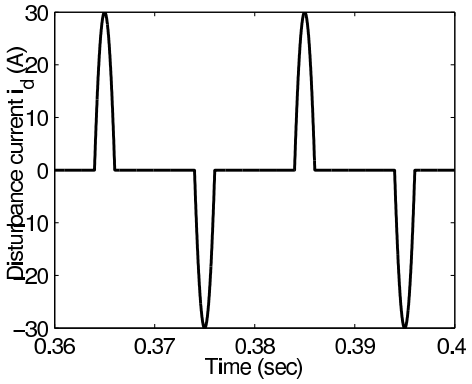

(a) The disturbance current i_d

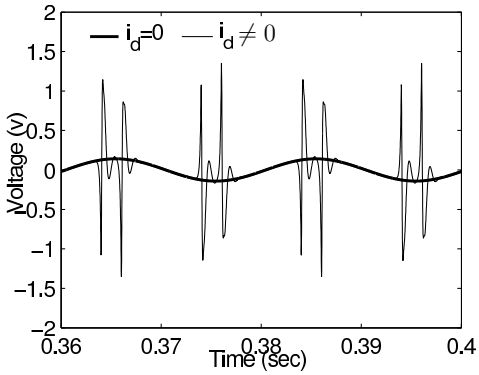

(b) The steady-state tracking error

Figure 7: The steady-state error for the nominal load with and without disturbance current (the PWM block and the inverter are modeled as a simple saturation)

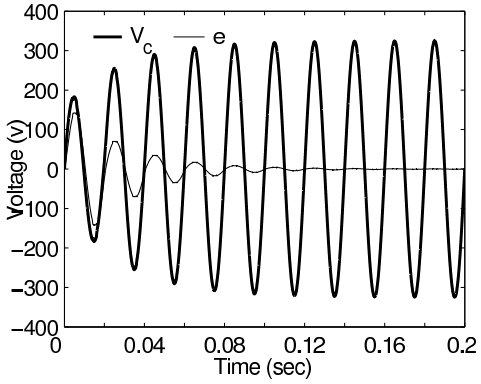

(a) The output voltage and the error

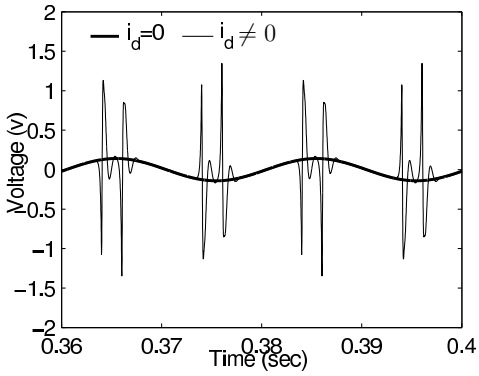

(b) The steady-state tracking error

Figure 8: The output voltage and the tracking error for a purely resistive load of 50Ω with and without the disturbance current shown in Figure 7(a) (the PWM block and the inverter are modeled as a simple saturation)

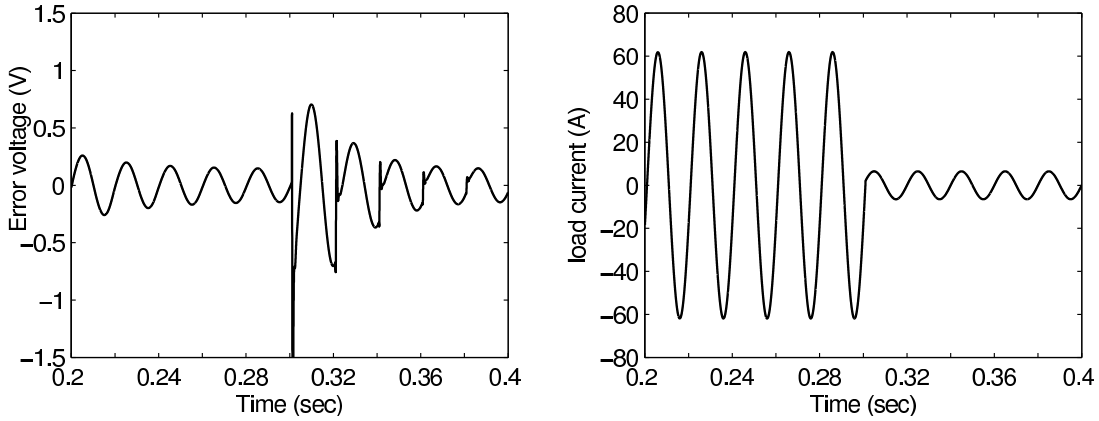

(a) The tracking error voltage (b) The load current

Figure 9: The transient response when the load is changed at $t = 0.301$ sec from the nominal load (as in Figure 1) to a resistor of 50Ω. There is no disturbance current and the PWM block and the inverter are modeled as a saturation.

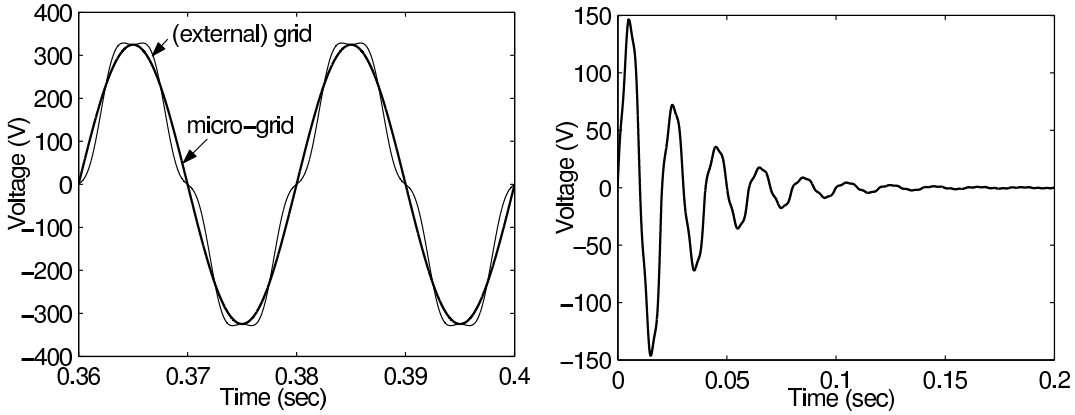

(a) The grid voltages (b) The transient tracking error

Figure 10: The effect of a distorted public grid: the grid voltages and the tracking error